ADVANCED QUANTUM TECHNOLOGIES
www.advquantumtech.com

Vacuum Field Photonic Trap for Excitons

Massimo Gurioli

The spectral and spatial dependence of the resonant Lamb shift of an exciton inside a photonic vacuum field landscape is considered to predict an optical dipole potential generated via virtual photons quantum fluctuations. This trapping potential can be exploited for exciton self-positioning in electric field hotspots at the nanoscale in view of quantum electrodynamics effects. By non Hermitian decomposition of the electromagnetic Green tensor in terms of quasi normal modes, the resonant part of the Lamb shift is expressed as Fano profile strictly interlinked to the Purcell enhancement of the exciton radiative lifetime. This approach explains how to tailor the depth of the vacuum photonic potential in several possible scenarios.

1. Introduction

In view of the development of future quantum technologies in semiconductor platforms, one of the main building blocks is certainly tailoring and controlling of the spontaneous emission of localized excitons.[1,2] This is of utmost importance for quantum cryptography, quantum sensors, quantum communication, and quantum computing. Such applications rely on the manipulation of an exciton, acting as an artificial atom and on the exploitation of the quantum nature of the emitted light, for generation of single as well as entangled photons.[1,2] Recent developments in nanophotonics led to unprecedented control of the spontaneous emission by tailoring the exciton dielectric landscape.[3–5] In parallel to the experimental efforts, theoretical understanding of the fundamental interaction mechanisms of exciton and photon also becomes more and more essential for proposing new schemes of manipulation of quantum emitters.

Controlling light–matter interaction at the nanoscale requires a spectral and spatial matching between the localized exciton and the photon mode.[6] The need to confine the exciton at an antinode of the electric field of a photonic resonator, with a resolution of few tens of nm, is a very difficult technological challenge debated for decades. It was eventually solved by nano-fabricating the photonic cavity around a bright semiconductor quantum dot (QD),[6,7] by site controlled QDs growth,[8] or by creating the QD in a prefabricated cavity.[9] Other approaches have been recently proposed such as the localization of 2D excitons via focused Gaussian beams in fiber Bragg mirror,[10] and in situ tuning microcavity devices, both in frequency and in lateral position with a movable external top mirror.[11] These efforts demonstrate the relevance of the goal and the need to still pursue new ideas.

All these approaches are quite complicated and hard to be scaled for a realistic device on a chip. Our idea is quite different: we propose to exploit a vacuum field optical photonic trap that is able to self-localize excitons in hot spot of vacuum electric field, via the resonant part of the exciton Lamb shift. We limit our model to the weak-coupling regime, where being able to self-trap an exciton while simultaneously tailoring its optical properties (photon antibunching, enhanced radiative rate, and light extraction) will be of relevance for a large variety of quantum devices.

2. General Discussion

2.1. Optical Traps

Using light to confine and move atoms, molecules and dielectric particles has been an extremely successful experimental tool in a huge variety of research fields, leading to three Nobel awards: optical tweezers, cooling and trapping neutral atoms, Bose Einstein condensation. A fascinating niche of optical forces, not yet fully explored, is related to mechanical effects of the electromagnetic vacuum quantum field.[12] The most famous example is the force between two mirrors, forming a planar optical cavity. The change in the electromagnetic density of states inside the cavity determines a deficit of quantum creation and annihilation of virtual photons. The net imbalance of the vacuum radiation force on the inner and external sides of each mirror creates the famous attractive Casimir force.[13,14] Other examples are the Casimir Polder potential between a single ground-state atom and other bodies,[15,16] which is due to the part of the Lamb-shift which depends on the atomic position.[17]

Much less, if nothing, has been done on vacuum optical potential for excitons, despite the strong similarity with atoms of these excited states of semiconductor physics. Exciton localization can be obtained in various way, the most relevant are epitaxial quantum dots (QDs), one of the most promising platform toward solid-state quantum emitters.[1,2] Owing to the electron–hole Coulomb interaction, confined excitons in 3 dimensions can

Prof. M. Gurioli
Department of Physics
University of Florence
via Sansone 1, Sesto Fiorentino, Florence I-50019, Italy
E-mail: massimo.gurioli@unifi.it

The ORCID identification number(s) for the author(s) of this article can be found under https://doi.org/10.1002/qute.202100046

DOI: 10.1002/qute.202100046

be considered as artificial atoms and are very well described as two-level systems (TLS). In particular, quantum electrodynamics effects lead to relevant self-energy correction of the exciton states. The imaginary part of this correction, known as Purcell effect in weak coupling limit, has been quantitatively accounted by the TLS approximation for localized exciton state. For large exciton and photon interaction the perturbation approach fails and strong coupling occurs.[1,6] Despite the huge effort in photonic, plasmonic and meta-materials to tailor on demand the electromagnetic density of states,[3–5] little attention has been paid on the possibility to engineer the exciton Lamb shift, which comes out from the real part of the self-energy correction. Interestingly, for photonic and plasmonic resonators, the Lamb shift is convergent and there is no need for high frequency cut-off.[18] The role of Lamb shift for the formation of Wannier exciton-plasmon Polariton bound to metal nanoparticles has been proposed to attain the very strong coupling regime.[19] Recently an interesting study pointed out the possibility to tailor and increase the Lamb shift exploiting the non-Hermitian nature of the light matter interaction.[20]

We aim to manipulate and confine excitons in a quantum optical trap. This method would have the relevant advantage of not requiring the QD site control at the nanoscale and takes inspiration from the atom localization in laser optical trap. We demonstrate the link between the quantum radiative shift of the exciton energy with the classical optical trap on a neutral atom driven by laser standing waves (see also the Supporting Information). Therefore we propose to exploit the resonant Lamb shift to create a localized exciton automatically located in a region of relevant effect.[21] Moving to open systems, we derive an analytic formula for the resonant Lamb shift for an exciton in resonant interaction with the quasi normal mode (QNM) of a photonic cavity.[3] The radiative rate and resonant Lamb shift are described by interconnected Fano profiles associated to the complex nature of the modal volume.[3] Then the problem of designing the vacuum photonic potential for excitons is translated into the tailoring of the QNM phase, which we finally analyze in hybrid photonic configurations.

2.2. Exciton Lamb Shift

We consider the exciton as a two-level quantum emitter embedded in a photonic structure. The exciton will experience a modified decay rate γ^* and a Lamb shift of the emission frequency $\omega^* = \omega_X + \Delta\omega$, compared to the case of a homogeneous system denoted by γ_X and ω_X respectively. The standard formula for the Lamb shift is given by a principal value integral of the imaginary part of the Green's function with the proper kernel. This principal value integral can be decomposed into two parts by using Kramers–Kronig relations for the Green tensor.[22] One term involves the real part of the Green's tensor named "resonant part", and the other term is given by an integral over all frequencies, named "non-resonant part" or "van der Waals contribution". Following ref. [23], approximating the atomic structure as harmonic oscillator or TLS, the non-resonant part of the excited level shift cancels with the shift of the ground state, when calculating the energy of the optical transition. More generally and as discussed later on, for the aim of this paper the resonant part is the only relevant term; note that this part also corresponds to the classical limit for the Lamb shift.[23,24] This means that, within our scopes and without the need of any specific approximations for the exciton internal structure, γ^* and ω^* can be obtained by the imaginary and real part of the Green function (that is the Green tensor projected on the exciton dipole versor $\mathbf{u}$) at the position and at the frequency of the emitter.

Hereafter, we proceed to only consider the resonant term in the exciton Lamb shift. Furthermore, in most cases of interest in photonics, the exciton is in resonance with one or, at most, few QNMs. Then we can expand the Green function in terms of a sum over the relevant QNMs,[3] with normalized complex electric fields $\tilde{\mathbf{E}}_n(\mathbf{r})$ and complex frequencies $\tilde{\omega}_n = \omega_n - i\Gamma_n$, with ω_n the resonant frequency and Γ_n the coherence damping rate; the quality factor is $Q_n = \omega_n/2\,\Gamma_n$. Within these approximations and considering a nonmagnetic cavity (i.e., with $\mu(\mathbf{r}) = 1$), one leads to the following expressions for the exciton radiative rate and the resonant Lamb shift.[20]

$$\gamma^*(\omega_X, \mathbf{r}) \cong -\sum_n \frac{3\pi c^3 \gamma_X}{{\omega_X}^2 \varepsilon(\mathbf{r})^{3/2}} \mathrm{Im}\left(\frac{1}{\tilde{V}_n(\mathbf{r})} \frac{1}{(\omega_X - \omega_n) + i\Gamma_n}\right) \overset{\text{HL+SM}}{\Rightarrow} \frac{3\pi c^3 \gamma_X}{{\omega_X}^2 \varepsilon(\mathbf{r})^{3/2}} \frac{1}{|\tilde{V}_n(\mathbf{r})|} \left(\frac{\Gamma_n}{(\omega_X - \omega_n)^2 + {\Gamma_n}^2}\right) \tag{1}$$

$$\Delta\omega(\omega_X, \mathbf{r}) \cong \sum_n \frac{3\pi c^3 \gamma_X}{2{\omega_X}^2 \varepsilon(\mathbf{r})^{3/2}} \mathrm{Re}\left(\frac{1}{\tilde{V}_n(\mathbf{r})} \frac{1}{(\omega_X - \omega_n) + i\Gamma_n}\right) \overset{\text{HL+SM}}{\Rightarrow} \frac{3\pi c^3 \gamma_X}{2{\omega_X}^2 \varepsilon(\mathbf{r})^{3/2}} \frac{1}{|\tilde{V}_n(\mathbf{r})|} \left(\frac{(\omega_X - \omega_n)}{(\omega_X - \omega_n)^2 + {\Gamma_n}^2}\right) \tag{2}$$

Note the rate in Equation (1) refers to the population radiative rate and it is twice the coherent dipole rate (usually denominated $1/T_1$ and $1/T_2$, respectively). It is important to remark that $\tilde{\mathbf{E}}_n(\mathbf{r}) \cdot \mathbf{u}$ has to be properly normalized; here we use $\int 2\varepsilon_o \varepsilon(\mathbf{r})(\tilde{\mathbf{E}}_n(\mathbf{r}) \cdot \mathbf{u})^2 d\mathbf{r} = 1$ (see discussion in ref. [3]). Here we also use the definition $\tilde{V}_n(\mathbf{r}) = [2\varepsilon_o \varepsilon(\mathbf{r})(\tilde{\mathbf{E}}_n(\mathbf{r}) \cdot \mathbf{u})^2]^{-1}$;[3,25] note that a different normalization and definition of modal volume was used in ref. [20] (i.e., $\tilde{V}_n(\mathbf{r}) = [(\tilde{\mathbf{E}}_n(\mathbf{r}) \cdot \mathbf{u})^2]^{-1}$) which leads to apparent differences with Equations (1) and (2). In the left parts of both Equations (1) and (2), with the symbol $\overset{\text{HL+SM}}{\Rightarrow}$ we mean to apply the Hermitian limit (HL) and single mode (SM) case. We will discuss HL in presenting the data of **Figure 1**, while SM obviously means to only keep the n-th term of the summation.

While the single mode approximation in Equation (1) has been verified in many cases,[3] it is relevant discussing the validity of Equation (2) for estimating the excitonic Lamb shift in resonance with highly confined QNMs, that is for the standard situation in nano-photonics. The comparison have been done for spherical resonators, where analytical solutions for the full multimodal photonic Green's function exist.[20] The results of Equations (1) and (2) for specific (and quite lossy) QNM of spherical Mie and plasmonic resonators (they have $Q_n = 120$ and $Q_n = 15$, respectively, i.e., well outside the Hermitian limit), reflect all the

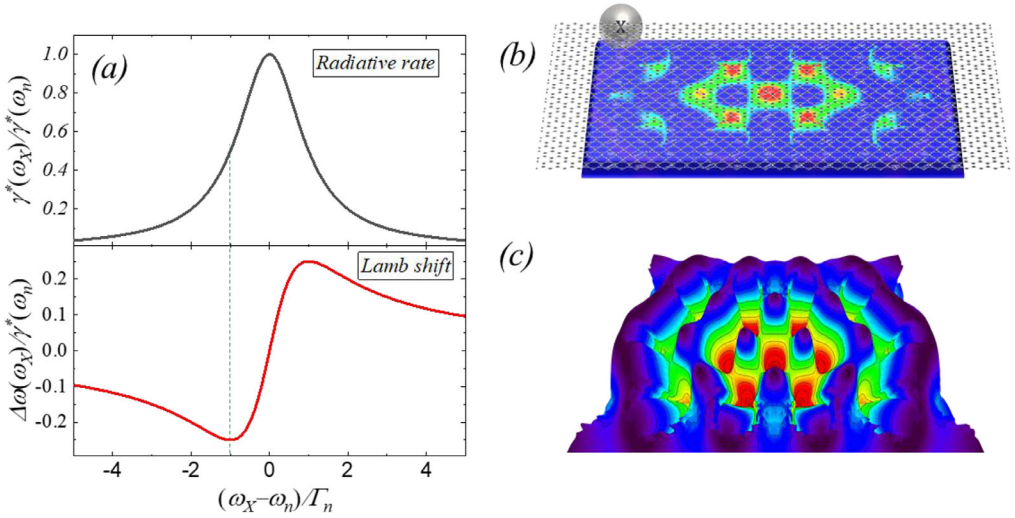

Figure 1. a) Spectral lineshape of radiative rate and resonant Lamb shift for an exciton within HL and SM limit. b) Scheme for the VPP in the case of a L3 photonic crystal cavity on slab. The map of the electric fields intensity is given in a scale color. On the slab we report a flake of 2D semiconductor, with a gray sphere representing the free exciton (not yet trapped). c) Expected VPP landscape for an exciton inside the 2D semiconductor material on the L3 cavity with resonant condition of $\omega_X = \omega_n - \Gamma_n$ (in a 3D rendering of the electric field intensity of (b)).

relevant features of the exact analytical resonant exciton Lamb shift, even if sizeable differences are found.[20]

A second important point is to discuss the validity of Equation (2) only considering the resonant term in the exciton Lamb shift. More generally, we have to include in Equation (2) the non-resonant term of the Lamb shift via an integral over all frequencies, which is quite complicated to evaluate. However, even for a quite lossy QNM of $Q_n \approx 100$ its resonance covers a spectral interval of only 5 nm in the visible range, while its spatial modulation occurs on a scale of about 100 nm. Assuming the non-resonant contribution of the Lamb shift as a constant value in space and frequency is a good approximation and it is certainly even better for non-lossy QNM of $Q_n > 1000$.

In summary, we are confident that Equation (2) is a good approximation for discussing the spectral and spatial dependence the exciton Lamb shift in nanostructured photonics systems. Anyway, to avoid confusion hereafter, we will refer to Equation (2) as the resonant exciton Lamb shift and use it as a powerful tool for understanding the physics underlying the idea of a vacuum photonic trap for an exciton in almost any relevant situations in nano-photonics. A derivation beyond this approximation is outside the scope of this contribution. Finally, we are considering dispersion less and non-magnetic media, which is valid for many semiconductors at frequency inside the electronic gap.

3. Vacuum Optical Trap

In the Hermitian limit of Equations (1) and (2), the field $\tilde{\mathbf{E}}_n(\mathbf{r}) \cdot \mathbf{u}$ is real to a very good approximation and then $\tilde{V}_n(\mathbf{r}) \cong |\tilde{V}_n(\mathbf{r})|$. This holds for a spectrally isolated n-th QNM with relatively high Q_n and then the expressions at the left of the limit $\overset{\text{HL+SM}}{\Rightarrow}$ in Equations (1) and (2) hold. To put some safe and realistic numbers, this is well verified for a spectrally isolated resonance in the local density of states with $Q_n > 500$. In this limit Equation (1) gives the textbook formula for the well-known Purcell formula, where $\gamma_n^*(\omega_X, \mathbf{r}_o)$ has a Lorentzian profile. The spectral dependence of $\gamma_n^*(\omega_X, \mathbf{r}_o)$ (at the position $\mathbf{r} = \mathbf{r}_o$ where $\tilde{V}_n(\mathbf{r})$ is minimum) is reported in Figure 1a, as a function of the normalized exciton detuning $\epsilon = (\omega_X - \omega_n)/\Gamma_n$. Obviously $\gamma^*_{\max} = \gamma_n^*(\omega_n, \mathbf{r}_o)$ is the maximum Purcell's enhanced radiative rate of the exciton for the selected QNM. The resonant exciton Lamb shift $\Delta\omega_n(\omega_X)$, normalized to $\gamma^*_{\max}$, is also reported for comparison.

The resonant Lamb shift is zero at $\omega_X = \omega_n$ and the exciton transition is blue (red) shifted for positive (negative) detuning ϵ, respectively. This result points out the presence of a photonic potential for the exciton $U_X(\mathbf{r}) = \hbar\Delta\omega_n(\mathbf{r}, \omega_X)$. The resulting potential $U_X(\mathbf{r})$ has the spatial distribution $|\tilde{\mathbf{E}}_n(\mathbf{r}) \cdot \mathbf{u}|^2$ and for $\omega_X < \omega_n$ it may localize the exciton. A formula similar to Equation (2) is used for the optical atomic trap, where however, the electric field is a laser standing wave; the comparison is discussed in the Supporting Information.

The potential $U_X(\mathbf{r})$ is a kind of Casimir–Polder effect for exciton. However, in order to avoid confusion with the broad band nature of the Lamb Shift for atoms, hereafter we will refer to $U_X(\mathbf{r})$ as vacuum photonic potential (VPP). The maximum VPP is $\mathbf{r} = \mathbf{r}_o$ and, within the Hermitian approximation of the QNM, its maximum depth is $\hbar\gamma_n^*(\omega_X = \omega_n - \Gamma_n, \mathbf{r}_o)/2$, occurring when $\omega_X = \omega_n - \Gamma_n$. Thus, the confining potential has the size of the hot spots of the electric field distribution (typically of the order of one tenth of the corresponding lambda in vacuum) and a depth which is 1/2 of the actual radiative rate for $\omega_X = \omega_n - \Gamma_n$. Note that $\gamma_n^*(\omega_X = \omega_n - \Gamma_n, \mathbf{r}_o)$ is also half of the maximum exciton radiative rate in the cavity $\gamma^*_{\max} = \gamma_n^*(\omega_X = \omega_n, \mathbf{r}_o)$, to which we will normalize all the values later on.

Several conditions are required to really trap the exciton within the VPP. In order to fix some numerical values, a localized exciton may have a radiative lifetime as small as of 100 ps.[26] Taking into account a photonic cavity with Purcell effect of about 50, leading to $1/\gamma^*_{\max} = 2$ ps, the trap depth would be 80 μeV which

corresponds to a temperature of 1 K. Since experimental temperatures as low as $T \cong 25$ mK is routinely used in semiconductor transport experiments, the condition that the depth of the confining potential must exceed the thermal energy, $\hbar\gamma^*_{\max}/4 > k_B T$ is experimentally obtainable. Moreover, the previous formulas hold in the weak coupling regime between exciton and photon, that is $\gamma^*_n(\omega_n, \mathbf{r}_o) < \Gamma_n$, which in the optical range roughly means $Q_n \lesssim 3000$. All together, these values are rather demanding, but also realistic in some selected systems.

Figure 1b reports a possible sketch of experimental realization of the vacuum optical trap for an exciton belonging to a 2D semiconductor layer leaned atop of a L3 photonic crystal cavity on slab. Excitons in these systems can be described as a TLS atomic-like system with center of mass (COM) degree of freedom (a gray sphere in Figure 1b), a model largely used in quantum well systems.[27–29] Due to the vacuum field fluctuations on the underlying photonic slab, the exciton COM will experience a potential landscape that is the vacuum field trap we are discussing. The concept that additional potential in a 2D landscape leads to exciton localization and quantum emitters has been largely validated in the quantum well physics.[28,29] It is also interesting to remark that similar concepts of trapping by photonic environment have been proposed for confining cold atoms on proximity of integrated devices, the so-called atom on chip.[30] However, there is the need of a 3D optical trap for localizing the atoms. The advantage of our approach is the natural exciton confinement in one direction in quantum well systems as in the emerging class of 2D semiconductor materials or perovskite nano-layers, requiring a much simpler VPP in only 2 dimensions. Similarly, for excitons in quantum wires or carbon nanotubes a 1 dimension VPP would be likely enough.

The spatial modulation of $U_X(\mathbf{r})$ (i.e., $|(\tilde{\mathbf{E}}_n(\mathbf{r})\cdot\mathbf{u})|^2$) is also sketched as a 3D profile in Figure 1c for the same L3 photonic crystal cavity of Figure 1b, to visualize the exciton potential landscape. In this case, the trap size is of the order 100 nm (for exciton transition in the near infrared, that is lambda in vacuum around 1300 nm), which is large enough to neglect additional quantum confinement that would push the exciton at higher energy. It is worth stressing that excitons will also experience an enhancement of their radiative rate of the order of one fourth of the maximum Purcell effect in the selected cavity, around 10 in our examples so still relevant. Finally, in view of quantum-light emitters, we could expect that the Coulomb and exchange interactions between two excitons within 100 nm should be strong enough to avoid degeneracy between the two excitons, leading to single photon emission as well as entangled photon via biexciton-exciton cascade.[1]

Several experimental benchmarks of the exciton self-trapping may be imagined, such as to spatially monitor the position of the emitter via confocal microscope and/or super-resolution combined with the check of single photon emission via antibunching experiments. Finally, it is worth mentioning that we are skipping the kinetics of trapping the exciton in the VPP, which is likely quite complicated since the exciton equations describe a non-linear problem. This is largely beyond the scope of this contribution. However, we may suggest the resonant excitation with high spatial resolution in order to create the exciton already inside the photonic trap, as an experimental configuration able to circumvent the dynamics of exciton localization process.

3.1. Non Hermitian Systems

Moving on, we aim to exploit the predictions of Equations (1) and (2) in open systems when, accordingly with non-Hermitian models, $\tilde{V}_n(\mathbf{r})$ is complex. This allows us to tailor the resonant exciton Lamb shift by special photonic design for enhancing the VPP for exciton. This aspect has been already discussed in ref. [20] in terms of the complex modal volumes showing that the limit $\hbar\gamma^*_n(\omega_X, \mathbf{r}_o)/2$ for maximum resonant Lamb shift can be overcome. This result can be easily understood by formulating Equations (1) and (2) in terms of Fano asymmetry parameters, following the approach of ref. [31]. It is lengthy but straightforward (see Supporting Information) to show (here: $\epsilon = (\omega_X - \omega_n)/\Gamma_n$)

$$\gamma^*(\omega_X, \mathbf{r}) = \sum_n \gamma^*_n(\omega_X, \mathbf{r}) = \sum_n \frac{6\pi c^3 \varepsilon_o}{\omega_X{}^2 \varepsilon(\mathbf{r})^{1/2}} \gamma_X \frac{\left|(\tilde{\mathbf{E}}_n(\mathbf{r})\cdot\mathbf{u})\right|^2}{\Gamma_n} F_{q_n(\mathbf{r})}(\epsilon) \tag{3}$$

$$\Delta\omega(\omega_X, \mathbf{r}) = \sum_n \Delta\omega_n(\omega_X, \mathbf{r}) = -\sum_n \frac{3\pi c^3 \varepsilon_o}{\omega_X{}^2 \varepsilon(\mathbf{r})^{1/2}} \gamma_X \frac{\left|(\tilde{\mathbf{E}}_n(\mathbf{r})\cdot\mathbf{u})\right|^2}{\Gamma_n} F_{q'_n(\mathbf{r})}(\epsilon) \tag{4}$$

$$F_q(\epsilon) = \frac{1}{(q^2+1)}\left(\frac{(q^2-1)+2q\epsilon}{1+\epsilon^2}\right) \tag{5}$$

where $F_q(\epsilon)$is the normalized expression for a Fano profile, which has zero background, i.e. the Fano profile goes to zero for $\epsilon \to \pm\infty$. Moreover $F_q(\epsilon)$ has, for any finite value of q, a zero crossing at $\epsilon = (1-q^2)/2q$, two extrema at $\epsilon = q$ and $\epsilon = 1/q$ and the amplitude between them is 1, for any value of q. Important symmetry relations of this function are $F_{-q}(\epsilon) = F_q(-\epsilon)$ and $F_{1/q}(\epsilon) = -F_{-q}(\epsilon) = -F_q(-\epsilon)$. Note that Equation (3) has been already derived, discussed and experimentally demonstrated in ref. [31]; Equation (4) is a natural and yet novel extension, its predictions are discussed hereafter (more details are given in Supporting Information).

The two Fano parameters $q_n(\mathbf{r})$ and $q'_n(\mathbf{r})$ for Purcell effect and resonant Lamb shift are interconnected, both associated to the spatial phase of the n-th QNM, which is fully defined by the normalization and it is a physical observable.[25,31]

$$q_n(\mathbf{r}) = -\frac{\mathrm{Re}\left[(\tilde{\mathbf{E}}_n(\mathbf{r})\cdot\mathbf{u})\right]}{\mathrm{Im}\left[(\tilde{\mathbf{E}}_n(\mathbf{r})\cdot\mathbf{u})\right]};\ q'_n(\mathbf{r}) = -\frac{1-q_n(\mathbf{r})}{1+q_n(\mathbf{r})} \tag{6}$$

For $q_n(\mathbf{r}) \to \infty$ we have $q'_n(\mathbf{r}) \to 1$ and the function $F_{q_n}(\epsilon)$ ($F_{q'_n}(\epsilon)$) is a Lorentzian (symmetric Fano) profile; in this case the two quantities $\hbar\gamma^*_n(\omega_X, \mathbf{r}_o)$ and $\Delta\omega_n(\omega_X, \mathbf{r}_o)$ are given by Figure 1a as a function of the normalized detuning $\epsilon = (\omega_X - \omega_n)/\Gamma_n$.

Equation (4) agrees with recent findings showing that the two Hermitian limits $|\Delta\omega_n(\omega_X, \mathbf{r}_o)| \le \gamma^*_{n,\max}/4$ and $|\Delta\omega_n(\omega_X, \mathbf{r}_o)| \le \gamma^*_n(\omega_X, \mathbf{r}_o)/2$ can be overcome.[20] Indeed we have demonstrated that keeping fix all the other parameters but $q_n(\mathbf{r})$, the maximum resonant Lamb shift for a single QNM is bounded $\gamma^*_{n,\max}/4 \le$

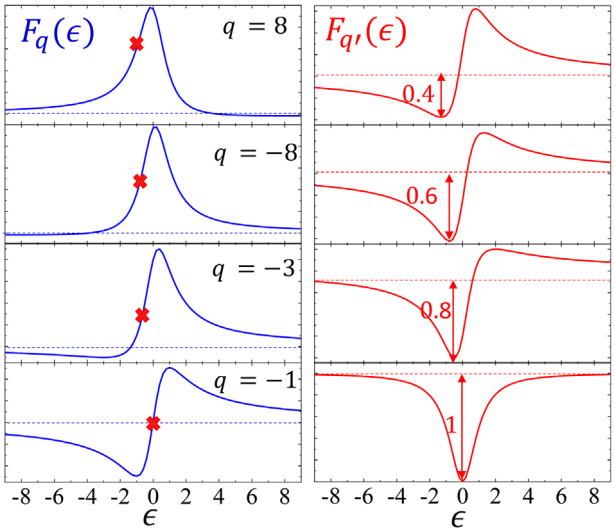

Figure 2. Radiative rate (left panels and blue lines) and resonant Lamb shift (right panels and red lines) from Equations (3) and (4) for different values of q (then $q' = -(1-q)/(1+q)$). The dashed lines indicate the zero amplitude. In all plots the total extension of the vertical axis is 1.1; note also that the peak to dip amplitude of the normalized Fano profiles is always 1. The values of q are given in the left panels, as well as the values of the dips in $F_{q'}(\epsilon)$ (i.e., of the exciton trap depth) in the right panels. The red crosses in the left panels give the position of dips in $F_{q'}(\epsilon)$ to highlight the variation of the Purcell effect for excitons in the trap.

$|\Delta\omega_{n,\max}| \leq \gamma^*_{n,\max}/2$; the upper limit holds for $q_n(\mathbf{r}) = \pm 1$ where also $|\Delta\omega_n(\omega_X, \mathbf{r}_o)|/\gamma^*_n(\omega_X, \mathbf{r}_o) \to \infty$ for $\omega_X \to \omega_n$. A panorama of interlinked Fano lineshapes of the radiative rate and resonant Lamb shift (i.e., $F_q(\epsilon)$ and $F_{q'}(\epsilon)$ for different values of $q = q_n$ and $q' = q'_n$, keeping constant all the other parameters, is given in **Figure 2**. For $q > 20$ the Hermitian limit with Lorentzian-like Purcell effect (i.e., Figure 1a and $q = \infty$) is already a very good approximation

In order to optimize the exciton trap we note that for $q > 0$ (see the top panel of Figure 2 with $q = 8$) the maximum resonant Lamb shift corresponds to a blue shift of the excitonic transition. This acts as a potential barrier for the excitons, whereas the well potential at the opposite exciton detuning is even smaller than the Hermitian limit $\gamma^*_{n,\max}/2$. The general scenario given in Figure 2 shows that for deepening the well potential beyond the Lorentzian limit, negative values of q are necessary. Indeed whenever $q \to -q$, it follows $q' \to 1/q'$ and $F_{1/q'}(\epsilon) = -F_{q'}(-\epsilon)$, transforming a pronounced barrier for positive detuning in a pronounced well for negative detuning. Note also that the best trap would be realized for $q \to -1$ where $F_{q'}(\epsilon)$ is a Lorentzian dip of amplitude -1, but obviously we need to discuss the meaning of $\gamma^*_n < 0$, which looks unphysical.

From Equation (3) (and Figure 2) follows that $\gamma^*_n(\omega_X, \mathbf{r})$ shows negative values in some frequency region for any value of $|q_n| < \infty$. The constraint that $\gamma^*_n(\omega_X, \mathbf{r}) \geq 0$ for any exciton transition energy ω_X, when assuming Equation (3) to be exact, gives the conclusion that $[(\tilde{\mathbf{E}}_n(\mathbf{r}) \cdot \mathbf{u})^2]$ has to be real and only the Hermitian limit seems physical. The relevant missing part in Equations (3) and (4), is that any resonance in photonics is embedded in a continuum of states, meaning that any photonic mode is intrinsically a resonant state of an open system. On one side this implies that $\gamma^*_n(\omega_X, \mathbf{r})$ has a Fano profile. On the other side, it also unavoidably requires the presence of a continuum background of leaky states. It always turns out that the sum of the Fano profiles and this background gives a total positive radiative rate. These leaky states give a flat spectral background to the resonant exciton Lamb shift and radiative rate, leaving their spectral modulation defined by the QNM properties from Equations (3) and (4). Coming back to the exciton VPP described by Equation (4), it is important to stress that properties of the continuum define the Fano parameters q_n and q'_n in a subtle and yet not fully addressed way, as discussed hereafter.

3.2. Hybrid Systems

We know that for optimizing the exciton VPP, one needs to tailor and control q_n and we expect this to be possible by engineering the properties of the continuum. A general discussion of this is beyond the scope of this work. Here we propose a simple way to understand the main points by analyzing a much simpler and yet related case, that is a hybrid system of a low Q plasmonic nano-antenna coupled with a high Q photonic microcavity.[32] These systems were recently addressed as a viable method to profit from both the small modal volume of plasmonic resonator and the high Q of the photonic microcavities. At the same time, we reckon that the very lossy plasmonic QNM acts as an effective background continuum of states for the high Q cavity, so we expect to understand some general rules linking the features of the continuum with the resulting value of q_n and q'_n of the n-th QNMs of a photonic system in Equations (3) and (4).

Hybrid systems are a particular case of the well-known problem of coupling two QNMs. It has been shown that for two coupled QNMs of unbalanced losses, the imaginary part of the modal volumes can be large even for very high Q.[31] In addition this relevant non-Hermitian effect can be quantitatively predicted with an analytic coupled mode theory.[31] Starting from these results, here we extend the coupled mode theory to the hybrid systems with quite large detuning by benchmarking it via FDTD simulations (see Supporting Information).

We consider two mono-mode cavities with uncoupled complex eigen frequency $\tilde{\omega}_j = \omega_j - i\Gamma_j$ (frequency ω_j and loss rate Γ_j) ($j = 1, 2$); the cavities are coupled via a field tunneling rate g (here g is a real number). Then the two coupled QNM eigenvalues are $\tilde{\omega}_{\pm} = \omega_{\pm} - i\,\Gamma_{\pm} = \frac{1}{2}(\tilde{\omega}_1 + \tilde{\omega}_2) \pm \frac{1}{2}\tilde{\Omega}$ with $\tilde{\Omega} = \sqrt{(\tilde{\omega}_1 - \tilde{\omega}_2)^2 + 4g^2}$ being the complex frequency splitting. Hereafter, the quantities related to two QNMs of the coupled system are labelled by "+" and "−", whereas those related to the uncoupled cavity modes are labelled with "1" and "2". It has been shown that, when only the cavity #j (being $j = 1$ or 2) is driven by P_j, the spectral dependence of $\mathrm{Im}(c_j/P_j)$ (c_j represents the electric field amplitude inside the j-th cavity) is representative of the $\gamma^*(\omega_X, \mathbf{r}_j)$ lineshapes at the at the antinodes $\mathbf{r}_j$ of cavity #j.[31] In addition, the coupled mode theory also gives the correct expression for the complex modal volumes of the QNM. Therefore (see the Supporting Information), we use the spectral dependence of $\mathrm{Re}(c_j/P_j)$ to predict the resonant Lamb shift $\Delta\omega(\omega_X, \mathbf{r}_j)$ lineshapes.

With this analytical model we can easily analyze directly many different systems. In particular the dependence of radiative rate

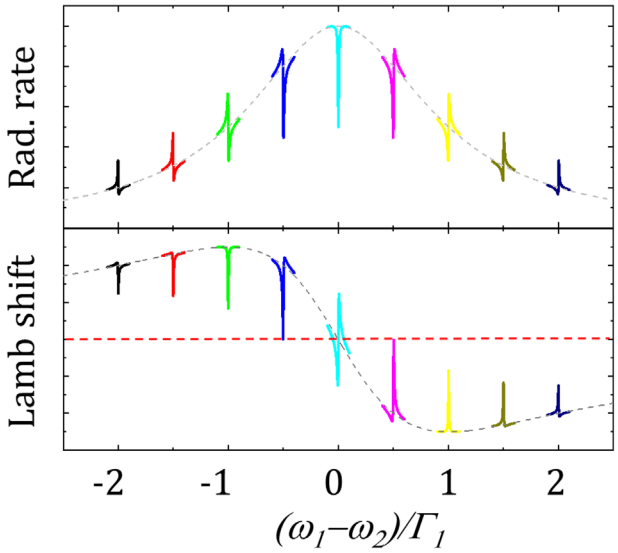

Figure 3. Radiative rate (top panel) and resonant Lamb shift (bottom panel) inside cavity #1 for different detuning between the optical modes in cavity #1 and #2 following Equations (4) and (5) (with different colors for different detunings ($\Delta = (\omega_1 - \omega_2)/\Gamma_1$)). The dashed gray lines give the broad background modulation associated with the lossy QNM in cavity #1, which is the same for all detunings. The red dashed lines are the zero in both plots. The colored lines are the sharp features in radiative rate and resonant Lamb shift in the coupled QNM, which spectrally move following the cavity detuning Δ. The detuning is varied at steps of 0.5.

and resonant Lamb shift inside cavity #1 on detuning between the two modes ($\Delta = (\omega_1 - \omega_2)/\Gamma_1$) is given in **Figure 3**, using different colors for the sharp features at different detuning. Note the full variety of Fano profiles for $\gamma^*(\omega_X, \mathbf{r}_j)$ when changing the detuning and the fact that in all cases $\gamma^*(\omega_X) > 0$ in the whole frequency range, as due to the "background" of the lossy plasmonic QNM. We found that for large positive Δ (as for $\Delta = 2$) the coupled mode predictions for $\gamma^*(\omega_X, \mathbf{r}_j)$ and $\Delta\omega(\omega_X, \mathbf{r}_j)$ show the similar spectral features obtained in ref. [20] for a spherical Mie resonator, that is a Fano profiles with more pronounced positive resonant exciton Lamb shift with respect to the negative shift. We also discover that for negative Δ it is possible to reverse the sign of Fano parameter, so enhancing the VPP beyond the Hermitian limit. To complete the analysis, we see that the case $q_n \approx 0$ can be obtained near zero cavity detuning $\omega_1 \approx \omega_2$ (pale blue lines in Figure 3) and the case $q_n = 1$, which gives the deepest exciton VPP, is for $\Delta = -1$ (green lines in Figure 3). More generally, for $\Gamma_1 \gg \Gamma_2$, the coupled mode model predicts the following simple relation $q_n \cong -\Delta = -(\omega_1 - \omega_2)/\Gamma_1$.

Our findings show that hybrid systems could be promising for demonstrating the VPP for excitons. Extrapolating these results to the case of a true continuum of states, we aim to point out some insights on how the Fano profiles in Equations (3) and (4) depends on the shape of a dispersive-like continuum. In particular we note in Figure 3 that $q_n > 0$ when the continuum density of states is increasing with the exciton frequency, which is indeed the standard case.[20] This finding brings us to suggest that for having $q_n < 0$, a continuum density of states decreasing with the photon frequency seems to be necessary. More generally, we believe that the control of the dispersion of the continuum would be an important key factor to tailor the VPP. A nice example of how the engineering of the continuum can tailor the photonic local density of states can be found in ref. [33], where coupling a cavity in a slow light wave guide led to large imaginary parts of the complex modal volume for a single photonic QNM.

4. Conclusions

In summary, we have shown that, within the weak coupling regime, photonics systems allow to realize a vacuum optical trap for excitons exploiting the same concepts leading to Casimir–Polder potential for neutral atoms. The advantage of a photonic system is not only to be able to trap an exciton but simultaneously to tailor its optical properties (photon antibunching, enhanced radiative rate and light extraction) for a new generation of quantum emitters. The great knowledge acquired by the photonic community for controlling the local density of states can then be used to design optimized VPP. In this scenario, the non Hermitian description of optical resonators offers a powerful tool to drive this research by tailoring the dispersion of the continuum. We believe that a lot of room for optimizing the exciton VPP is available in meta materials and in particular left-handed and topological materials, where exotic light behavior can be likely designed.

Supporting Information

Supporting Information is available from the Wiley Online Library or from the author.

Acknowledgements

The authors acknowledge useful and relevant discussions with Dr. Emmanuel Lassalle and funding from CdR Firenze (2018/24257).

Conflict of Interest

The author declares no conflict of interest.

Data Availability Statement

The data that support the findings of this study are available from the corresponding author upon reasonable request.

Keywords

exciton traps, Purcell effect, quantum emitters

Received: March 19, 2021
Revised: May 9, 2021
Published online: May 27, 2021

[1] A. J. Shields, *Nat. Photonics* **2007**, *1*, 215.
[2] M. Gurioli, Z. Wang, A. Rastelli, T. Kuroda, S. Sanguinetti, *Nat. Mater.* **2019**, *18*, 799.

[3] a) C. Sauvan, J. P. Hugonin, I. S. Maksymov, P. Lalanne, *Phys. Rev. Lett.* **2013**, *110*, 237401; b) P. Lalanne, W. Yan, K. Vynck, C. Sauvan, J.-P. Hugonin, *Laser Photonics Rev.* **2018**, *12*, 1700113.
[4] M. Pelton, *Nat. Photonics* **2015**, *9*, 427.
[5] R. Carminati, A. Cazé, D. Cao, F. Peragut, V. Krachmalnicov, R. Pierrat, Y. De Wilde, *Surf. Sci. Rep.* **2015**, *70*, 1.
[6] K. Hennessy, A. Badolato, M. Winger, D. Gerace, M. Atatüre, S. Gulde, S. Fält, E. L. Hu, A. Imamoğlu, *Nature* **2007**, *445*, 896.
[7] A. Dousse, L. Lanco, J. Suffczyński, E. Semenova, A. Miard, A. Lemaître, I. Sagnes, C. Roblin, J. Bloch, P. Senellart, *Phys. Rev. Lett.* **2008**, *101*, 267404.
[8] J. Große, M. von Helversen, A. Koulas-Simos, M. Hermann, S. Reitzenstein, *APL Photonics* **2020**, *5*, 096107.
[9] M. Felici, G. Pettinari, F. Biccari, A. Boschetti, S. Younis, S. Birindelli, M. Gurioli, A. Vinattieri, A. Gerardino, L. Businaro, M. Hopkinson, S. Rubini, M. Capizzi, A. Polimeni, *Phys. Rev. B* **2020**, *101*, 205403.
[10] A. Delteil, T. Fink, A. Schade, S. Höfling, C. Schneider, A. İmamoğlu, *Nat. Mater.* **2019**, *18*, 219.
[11] D. Najer, I. Söllner, P. Sekatski, V. Dolique, M. C. Löbl, D. Riedel, R. Schott, S. Starosielec, S. R. Valentin, A. D. Wieck, N. S. Sangouard, A. Ludwig, R. J. Warburton, *Nature* **2019**, *575*, 622.
[12] J. Y. Buhmann, *Dispersion Forces I*, Springer Tract in Modern Physics, Vol. *247*, Springer-Verlag, Berlin, Germany **2012**.
[13] H. B. G. Casimir, *Proc. K. Ned. Akad. Wet.* **1948**, *51*, 793.
[14] E. M. Lifshitz, *Sov. Phys. JETP* **1956**, *2*, 73.
[15] H. B. G. Casimir, D. Polder, *Phys. Rev.* **1948**, *73*, 360.
[16] S. Y. Buhmann, D. T. Ho, L. Knöll, D. G. Welsch, *Phys. Rev. A* **2004**, *70*, 052217.
[17] W. E. Lamb, R. C. Retherford, *Phys. Rev.* **1947**, *72*, 241.
[18] E. A. Muljarov, W. Langbein, *Phys. Rev. B* **2016**, *94*, 235438.
[19] J. B. Khurgin, *Nanophotonics* **2019**, *8*, 629.
[20] E. Lassalle, N. Bonod, T. Durt, B. Stout, *Opt. Lett.* **2018**, *43*, 1950.
[21] E. M. Purcell, H. C. Torrey, R. V. Pound, *Phys. Rev.* **1946**, *69*, 37.
[22] a) J. Wylie, J. Sipe, *Phys. Rev. A* **1985**, *32*, 2030; b) E. A. Hinds, V. Sandodhar, *Phys. Rev. A* **1991**, *43*, 398.
[23] E. Lassalle, A. Devilez, N. Bonod, T. Durt, B. Stout, *J. Opt. Soc. Am. B* **2017**, *34*, 1348.
[24] L. Novotny, B. Hetch, *Principles of Nano-Optics*, Cambrigde Press, Cambridge, UK **2012**.
[25] K. G. Cognée, W. Yan, F. La China, D. Balestri, F. Intonti, M. Gurioli, A. F. Koenderink, P. Lalanne, *Optica* **2019**, *6*, 269.
[26] P. Tighineanu, R. S. Daveau, T. B. Lehmann, H. E. Beere, D. A. Ritchie, P. Lodahl, S. Stobbe, *Phys. Rev. Lett.* **2016**, *116*, 163604.
[27] S. Glutsch, F. Bechstedt, *Phys. Rev. B* **1994**, *50*, 7733.
[28] V. Savona, C. Piermarocchi, A. Quattropani, F. Tassone, P. Schwendimann, *Phys. Rev. Lett.* **2001**, *87*, 076801.
[29] F. Intonti, V. Emiliani, C.h. Lienau, T. Elsaesser, V. Savona, E. Runge, R. Zimmermann, R. Nötzel, K. H. Ploog, *Phys. Rev. Lett.* **2001**, *87*, 076801.
[30] M. Keil, O. Amit, S. Zhou, D. Groswasser, Y. Japha, R. Folman, *J. Mod. Opt.* **2016**, *63*, 1840.
[31] D. Pellegrino, D. Balestri, N. Granchi, M. Ciardi, F. Intonti, F. Pagliano, A. Yu. Silov, F. W. Otten, T. Wu, K. Vynck, P. Lalanne, A. Fiore, M. Gurioli, *Phys. Rev. Lett.* **2020**, *124*, 123902.
[32] a) H. M. Doeleman, E. Verhagen, A. F. Koenderink, *ACS Photonics* **2016**, *3*, 1943; b) H. M. Doeleman, C. H. D. Dieleman, C. H. Mennes, B. Ehrler, A. Femius Koenderink, *ACS Nano* **2020**, *14*, 12027.
[33] R. Faggiani, J. Yang, R. Hostein, P. Lalanne, *Optica* **2017**, *4*, 393.